

Ly α Constraints on Very Low Luminosity AGN

Mark Dijkstra^{*} and J. Stuart B. Wyithe

School of Physics, University of Melbourne, Parkville, Victoria, 3010, Australia

2 December 2024

ABSTRACT

Recent surveys have detected Ly α emission from $z = 4.5 - 6.5$ at luminosities as low as 10^{41} erg s⁻¹. There is good evidence that low numbers of AGN are among observed faint Ly α emitters. Combining these observations with an empirical relation between the intrinsic Ly α and B-band luminosities of AGN, we obtain an upper limit on the number density of AGN with absolute magnitudes $M_B \in [-16, -19]$ at $z = 4.5 - 6.5$. These AGN are up to two orders of magnitude fainter than those discovered in the Chandra Deep Field, resulting in the faintest observational constraints to date at these redshifts. At $z = 4.5$, the powerlaw slope of the very faint end of the luminosity function of AGN is shallower than the slope observed at lower redshifts, $\beta_l < 1.6$, at the 99% confidence level. In fact, we find marginal evidence that the luminosity function rises with luminosity, corresponding to a powerlaw slope $\beta_l < 0$, at magnitudes fainter than $M_B \sim -20$ (76% confidence level). These results suggest either that accretion onto lower mass black holes is less efficient than onto their more massive counterparts, or that the number of black holes powering AGN with $M_B \gtrsim -20$ is lower than expected from the $M_{\text{BH}} - \sigma$ relation by one-two orders of magnitude. Extrapolating from reverberation-mapping studies suggests that these black holes would have $M_{\text{BH}} = 10^6 - 10^7 M_\odot$. To facilitate the identification of AGN among observed Ly α emitters, we derive observational properties of faint AGN in the Ly α line, as well as in the X-ray and optical bands.

Key words: cosmology: theory-quasars: general-galaxies: high redshift

1 INTRODUCTION

The quasar luminosity function (QLF) describes the space density of Active Galactic Nuclei (AGN) as a function of luminosity and redshift. The QLF encodes information on quantities like the black hole number density per unit mass, and the gas accretion efficiency. It therefore constrains physical models of AGN and of super massive black hole formation. The optical (B-band) QLF at $z \lesssim 4$ has been determined accurately for luminosities¹ exceeding $L_B \gtrsim 10^{11} L_{B,\odot}$ from the 2dF quasar survey (which corresponds to absolute magnitudes $M_B < -22$, Boyle et al. 2000; Croom et al. 2004). At higher redshifts the optical luminosity function of luminous quasars has been determined from quasars in the Sloan Digital Sky Survey (Fan et al. 2001) at $M_B \sim -27$. In addition, deep *Chandra* and *XMM* imaging has constrained the X-ray QLF at X-Ray luminosities as low as $L_X = 10^{42} - 10^{44}$ ergs s⁻¹ (Barger et al. 2003; Cowie et al. 2003; Hasinger et al. 2005). Following Haiman & Loeb (1998), Wyithe & Loeb (2003) have used the X-Ray QLF

to constrain the B-band QLF down to fainter optical luminosities ($M_B \sim -22$) at $z \gtrsim 4$. At these redshifts, no observational constraints exist on the optical QLF at fainter luminosities. However, the details of the existence and evolution of low luminosity AGN is crucial for our understanding of the growth of low mass black holes, and of their role in the formation of super massive black holes.

In this paper we demonstrate how existing Ly α surveys may be used to constrain the B-Band QLF at absolute magnitudes as low as $M_B = -16$. Existing wide-field narrow-band surveys (e.g. Rhoads et al. 2000) are optimised to detect Ly α line emission from high-redshift galaxies, and in order to maximise their detection rate, deeply image fields as large as 1 deg² on the sky (e.g. Taniguchi et al. 2005). The combination of wide field and deep images, together with concentration on a strong emission line, rather than continuum, allows these wide-field narrow-band surveys to put stringent constraints on the number density of AGN with $M_B \sim -19$. Constraints on even fainter AGN are derived from deep spectroscopic surveys of regions around intermediate redshift clusters of galaxies, which offer an ultra-deep view into the high redshift universe ($z=4.5-6.7$) through strong gravitational lensing (with magnification factors of 10-1000, Santos et al. 2004).

^{*} E-mail: dijkstra@physics.unimelb.edu.au

¹ One solar B-Band luminosity, denoted by $L_{B,\odot}$, corresponds to 4×10^{32} ergs s⁻¹.

Throughout this paper, the terms AGN and quasar are interchangeable and refer to broad lined active galactic nuclei, also known as "Type I" AGN. The outline of this paper is as follows: In § 2 we relate the Ly α luminosity of a quasar to its B-band luminosity. In § 3 we summarise constraints on the number density of Ly α emitters at high redshift, and discuss the abundance of quasars among these sources. We show how this existing data constrains the faint end of the quasar luminosity function. In § 4 we calculate the observable Ly α properties of AGN and use these to physically interpret our results. We also model the appearance of faint AGN in the optical and X-ray bands. Finally, in § 5 we discuss the possible cosmological implications of our work, before presenting our conclusions in § 6. We use the *WMAP* cosmological parameters: $(\Omega_m, \Omega_\Lambda, \Omega_b, h, Y_{\text{He}}) = (0.3, 0.7, 0.044, 0.7, 0.24)$ (Spergel et al. 2003) throughout the paper.

2 THE RELATION BETWEEN LY α AND B-BAND LUMINOSITIES IN AGN.

There is a very simple relation between the Ly α and B-band luminosities of a quasar. The continuum flux density of a quasar may be denoted either by F_E (in units of $\text{erg s}^{-1} \text{cm}^{-2} \text{erg}^{-1}$) or F_λ (in units of $\text{erg s}^{-1} \text{cm}^{-2} \text{\AA}^{-1}$). These quantities are related by the equality $\lambda F_\lambda = E F_E$, where $E = h_p c / \lambda$ is the photon energy and h_p is Planck's constant. Assuming the Ly α line has an equivalent width EW, the Ly α luminosity of a quasar becomes

$$L_{\text{Ly}\alpha} = \text{EW } F_\lambda|_{\lambda=1200\text{\AA}} = \left(\frac{\text{EW}}{1200\text{\AA}}\right) [\lambda F_\lambda]_{\lambda=1200\text{\AA}}. \quad (1)$$

The B-band luminosity can be estimated from

$$L_B = \text{BW } F_\lambda|_{\lambda=4400\text{\AA}} = \left(\frac{800}{4400}\right) [\lambda F_\lambda]_{\lambda=4400\text{\AA}}, \quad (2)$$

where we assumed the B-band filter to be centered on $\lambda = 4400\text{\AA}$ with a width of BW = 800 \AA . The ratio of $L_{\text{Ly}\alpha}$ and L_B becomes

$$\frac{L_{\text{Ly}\alpha}}{L_B} = 5.5 \left(\frac{\text{EW}}{1200\text{\AA}}\right) \frac{[E F_E]_{\lambda=1200\text{\AA}}}{[E F_E]_{\lambda=4400\text{\AA}}}. \quad (3)$$

Sazonov et al. (2004) have computed the characteristic angle-averaged, broad-band spectral energy distribution of the typical quasar. They show that in the range $E = 1 - 10$ eV, $E F_E \propto E^\gamma$, with $\gamma = 0.4$. The exact value of γ varies between individual objects. Fan et al. (2001) found that at $z \sim 4.5$ the spread in γ could be represented by a Gaussian with $\sigma_\gamma \sim 0.3$ in their sample of 39 quasars.

The intrinsic Ly α equivalent width for AGN is uncertain. Charlot & Fall (1993) showed that AGN which are completely surrounded by neutral hydrogen gas have Ly α EWs of $827\alpha^{-1}(3/4)^\alpha\text{\AA}$, where α is the spectral index blueward of the Ly α line. According to the template of Sazonov et al. (2004), $\alpha = 1.7$, which yields $\text{EW} \sim 300\text{\AA}$. However, the observed Ly α EWs of bright AGN are typically in the range 50-150 \AA , which could be attributed to dust attenuation of the Ly α line (see Charlot & Fall 1993, and references therein) and/or scattering in the IGM (see § 4.1). Fan et al. (2001) represent the distribution of observed EW by a

Gaussian centered on $\text{EW} = 70\text{\AA}$, with $\sigma_{\text{EW}} = 20\text{\AA}$. Under the assumption that half of the emitted Ly α photons are scattered in the IGM (see § 4.1 for a justification of this number), the intrinsic distribution of EW should be centered on $\text{EW} = 140\text{\AA}$. To be conservative and to reflect our ignorance of the Ly α EW's of faint AGN, we assume σ_{EW} to be 50 \AA .

The distribution of the ratio $L_{\text{Ly}\alpha}/L_B$ was obtained via Monte-Carlo, under the assumption that: 1) the slope γ follows a Gaussian distribution with $\gamma = 0.4 \pm 0.3$; and 2) the Ly α equivalent width follows a Gaussian distribution with $\text{EW} = 140 \pm 50\text{\AA}$, which is truncated at $\text{EW} = 0$ and 600 \AA . The ratio $L_{\text{Ly}\alpha}/L_B$ and its 95% confidence interval are found to be

$$\frac{L_{\text{Ly}\alpha}}{L_B} = 1.0^{+1.8}_{-0.6}. \quad (4)$$

Thus, within the uncertainties we may approximate the Ly α luminosity of an AGN as being equal to its B-band luminosity.

3 CONSTRAINING THE FAINT END OF QLF USING LY α SURVEYS.

3.1 The Number Density of AGN at $z = 4.5 - 6.5$.

Several Ly α surveys have derived the number density, $n_{\text{Ly}\alpha}$, of Ly α emitters brighter than a minimum detectable Ly α luminosity, $L_{\text{Ly}\alpha, \text{c}}$. Examples include surveys at $z = 4.5$ (Dawson et al. 2004), $z = 5.7$ (e.g. Ouchi et al. 2005), $z = 6.5$ (Taniguchi et al. 2005) and $z > 4.5$ (Santos et al. 2004). These results are summarised in columns 1-4 in Table 1.

Since the detected Ly α emitters are generally identified as galaxies, the number density of quasars with $L_{\text{Ly}\alpha} > L_{\text{Ly}\alpha, \text{c}}$ must be smaller than $n_{\text{Ly}\alpha}$. Dawson et al. (2004) find that no AGN are among the Ly α emitters in their sample in a total comoving volume of $1.5 \times 10^6\text{ Mpc}^3$. This finding was based on the absence of broad line emitters in both their narrow band survey² and in follow-up high resolution spectra of 18 confirmed $z = 4.5$ Ly α emitters. Furthermore, these objects lacked high-ionization state UV emission lines, symptomatic of AGN activity. Additionally, deep X-Ray observations of 101 Ly α emitters by Wang et

² The survey volume of Dawson et al. (2004) is determined by 5 overlapping filters each of width 80 \AA , yielding a total wavelength coverage of 240 \AA . As will be demonstrated in § 4.1, the observed FWHM of the Ly α line of AGN at this redshift is typically $\sim 60 - 70\text{\AA}$, which implies that AGN would have been detected in more than two filters. From narrow-band imaging alone, Dawson et al. (2004) find no evidence for the presence of broad line emitters. If we represent the filter transmission curves with top hats of width 80 \AA , and an AGN's Ly α emission line with a Gaussian with a FWHM of 65 \AA , then on average $\sim 70\%$, 60% and 40% of the AGN's total Ly α flux is detected by three adjacent filters. This implies that 1) for an AGN to be detected in 1 filter at the 5- σ detection threshold, requires its Ly α flux to be $1/0.7 \sim 1.4$ times higher than the survey's detection threshold, and 2) for an AGN to be detected in 3 adjacent filters requires its peak flux to lie within the inner three narrow band filters. This reduces the survey volume in which these AGN can be identified by a factor of $(240 - 2 \times 40)/240 = 2/3$.

Table 1. Ly α Survey's Constraints on $n_{\text{Ly}\alpha}$ and the corresponding upper limits on $\Psi(L_{\text{B,min}}, z)$.

z	f_{min} (10^{-18} erg s $^{-1}$ cm $^{-2}$)	$L_{\text{Ly}\alpha, \text{c}}$ (10^{42} erg s $^{-1}$)	$n_{\text{Ly}\alpha}$ (10^{-4} Mpc $^{-3}$)	n_{AGN} (10^{-6} Mpc $^{-3}$)	$L_{\text{B,min}}$ $10^9 L_{\text{B}, \odot}$	$\Psi(L_{\text{B,min}}, z)$ (10^{-6} Gpc $^{-3}$ L $_{\text{B}}^{-1}$)
4.5 ¹	16	6	1.6	< 2	15	< 0.08 ($\beta = 1.0$)
5.7 ²	6	4	3.9	< 58	10	< 4 ($\beta = 1.6$)
6.6 ³	4.1	6	1.2	< 15	15	< 0.7 ($\beta = 1.6$)
> 4.5 ⁴	0.3	0.2	$10^{1.5}$	< $10^{4.1}$	0.5	< $10^{4.3}$ ($\beta = 1.6$)
> 4.5 ⁴	3.0	2	$10^{0.4}$	< $10^{2.8}$	5	< $10^{2.0}$ ($\beta = 1.6$)

(1) Data from Dawson et al. (2004). Note that the actual detection limit is quoted as $\sim 2 \times 10^{-17}$ erg s $^{-1}$ cm $^{-2}$. We have slightly revised their detection limit downwards, as 27% of their spectroscopically confirmed LAEs have a flux $< 2.0 \times 10^{-17}$ erg s $^{-1}$ cm $^{-2}$, with a mean flux of $\sim 1.1 \times 10^{-17}$ erg s $^{-1}$ cm $^{-2}$. As argued in § 3.1, the 5- σ detection threshold for AGN lies higher by a factor of 1.4 at $\sim 1.6 \times 10^{-17}$ erg s $^{-1}$ cm $^{-2}$.

(2) Data from Ouchi et al. (2005)

(3) Data from Taniguchi et al. (2005)

(4) From the deep spectroscopic survey of gravitationally lensed regions by Santos et al. (2004)

al. (2004, also see Malhotra et al. 2003), revealed no X-ray emission from any individual source at a 3- σ detection limit of $F_{0.5-10.0\text{keV}} = 6.6 \times 10^{-16}$ erg s $^{-1}$ cm $^{-2}$ (but this may not be that surprising as we discuss in § 4.3). The absence of AGN in the survey volume yields an upper limit on the number of AGN, $N_{\text{AGN}} \leq 3$ at the 95% confidence level.³

Similarly, Ouchi et al. (2005) found 515 objects within their survey volume of 1.3×10^6 Mpc 3 that are probable $z = 5.7$ Ly α emitters. Follow-up spectroscopy of 19 emitters revealed that their spectra are too narrow ($v_{\text{FWHM}} \lesssim 500$ km s $^{-1}$) to be AGN. If the sample of 515 detections contains a fraction of AGN, $f_{\text{AGN}} \lesssim 0.15$, then the probability that a random sample of 19 contains no AGN is $(1 - f_{\text{AGN}})^{19} \gtrsim 0.05$. This yields a 2- σ upper limit on the number of AGN, $N_{\text{AGN}} \lesssim 515 f_{\text{AGN}} = 75$.

Taniguchi et al. (2005) found 9 objects in their survey volume of 2×10^5 Mpc 3 that are likely to be $z = 6.5$ Ly α emitters. The line widths of their objects lie in the range 180-460 km s $^{-1}$. This, in combination with the lack of NIV $\lambda = 1640$ Å emission, strongly suggests no AGN are in their sample, yielding $N_{\text{AGN}} \leq 3$.

In their deep, blind, spectroscopic survey of regions that utilized strong-lensing magnification by $z = 0.2$ clusters of galaxies, Santos et al. (2004) found 3-5 Ly α emitting objects at $z > 4.5$ at unlensed flux levels as low as $\sim 3 \times 10^{-19}$ erg s $^{-1}$ cm $^{-2}$. The line widths of these sources are not reported, but Ellis et al. (2001) found the line width of one $z = 5.6$ Ly α emitter to be $\lesssim 100$ km s $^{-1}$, and is therefore unlikely an AGN. However, to be conservative, our upper limits are derived under the assumption that all these Ly α emitters could be AGN.

For each survey, we obtain upper limits on the number density of AGN from $n_{\text{AGN}} \lesssim N_{\text{AGN}} V_{\text{survey}}^{-1}$. The detection limit of each survey, f_{min} , is converted to its minimum Ly α detectable Ly α luminosity, $L_{\text{Ly}\alpha, \text{c}}$, using $L_{\text{Ly}\alpha, \text{c}} = 4\pi d_L^2(z) f_{\text{lim}} / (T)$. Here, $d_L(z)$ is the luminosity distance to redshift z and T is the mean transmitted Ly α flux from the AGN through the IGM. As will be discussed in § 4.1, we assume that for AGN $T = 0.5$ when $z < 6$ and $T = 0.3$ when

$z = 6.5$. Values of f_{lim} are given in Table 1. For the survey performed by Santos et al. (2004), the calculation of n_{AGN} is far more complicated, since both the detection limit and survey volume are functions of the position on the sky and of redshift. Fortunately, Santos et al. (2004) fully account for this and provide number densities of Ly α emitters with $L > L_{\text{crit}}$, for several values of L_{crit} . We obtain upper limits on n_{QSO} from the upper boundary of the 95% confidence levels on their quoted $n_{\text{Ly}\alpha}(L > L_{\text{crit}})$ for $\log[L_{\text{crit}}] = 41$ and 42 (their Figure 11. Our $L_{\text{Ly}\alpha, \text{c}} = 2L_{\text{crit}}$ because we account for 50% loss of flux in the IGM).

A summary of the minimum detectable Ly α luminosity, $L_{\text{Ly}\alpha, \text{c}}$ and our constraints on the number densities of AGN at $z = 4.5, 5.7$ and 6.5 is given in Table 1. By converting $L_{\text{Ly}\alpha, \text{c}}$ to a minimum B-band luminosity $L_{\text{B,min}}$ (Eq. 4), we are able to constrain the B-band QLF. This process is described in the following subsections.

3.2 Using the Number Density of AGN at $z = 4.5 - 6.5$ to Constrain the QLF.

The luminosity function $\Psi(L_{\text{B}}, z) dL_{\text{B}}$ is defined as the number of quasars per unit comoving volume having rest-frame B-band luminosities in the range between L_{B} and $L_{\text{B}} + dL_{\text{B}}$ at redshift z . The number density of AGN with $L_{\text{B}} > L_{\text{B,min}}$ is then given by

$$n_{\text{AGN}}(L_{\text{B}} > L_{\text{B,min}}; z) = \int_{L_{\text{B,min}}}^{\infty} \Psi(L_{\text{B}}, z) dL_{\text{B}} \quad (5)$$

To constrain the luminosity function at $L_{\text{B,min}}$ we must know the functional form of $\Psi(L_{\text{B}}, z)$, which is not constrained observationally at the redshift range of interest, $z \in [4.5, 6.5]$. We first constrain $\Psi(L_{\text{B}}, z)$ at $L_{\text{B,min}}$ at $z > 5$ under the assumption that the faint end of the quasar luminosity function observed at lower redshifts applies here as well. This is followed by a self-consistent constraint on $\Psi(L_{\text{B}}, z)$ and its slope at $z = 4.5$.

3.2.1 Constraints on $\Psi(L_{\text{B}}, z)$ at $z > 5$.

The following double power law provides a good representation of the observed quasar luminosity function at $z \leq 3$

³ This is because for a Poisson distribution $P(n, \mu) = e^{-\mu} \mu^n / n!$ with an expected number of events $\mu = 3.0$, the probability of having more than 0 events occur is 95%.

(Boyle et al. 2000)

$$\Psi(L_B, z) = \frac{\Psi_*/L_*(z)}{\left(\frac{L_B}{L_*(z)}\right)^{\beta_h} + \left(\frac{L_B}{L_*(z)}\right)^{\beta_l}}. \quad (6)$$

The slope at the bright and faint end of the luminosity function is $\beta_h = 3.52$ and $\beta_l = 1.66$, respectively. All redshift dependence lies in the transition luminosity $L_*(z)$. If the same parameterization holds at $z > 5$ and $L_{B,\min} \ll L_*(z)$, then the integral in Eq (5) is dominated by the faint end of the luminosity function and the β_h -term may be omitted. Eq (5) then becomes

$$n_{\text{AGN}}(L_B > L_{B,\min}; z) = \frac{L_{B,\min}}{\beta_l - 1} \Psi(L_{B,\min}, z), \quad (7)$$

which shows that the upper limit on $n_{\text{AGN}}(L_B > L_{B,\min}; z)$ translates directly to an upper limit on $\Psi(L_{B,\min}, z)$. These constraints are summarised in the last column of Table 1 (at $z = 5.7$ and $z = 6.5$). In Figure 1 we compare the above constraint on the quasar B-band luminosity function (denoted by the *filled circles* at $\log[L_B/L_{B,\odot}] \lesssim 10$ in central and right panel), with data at higher luminosities. Each panel corresponds to the redshift printed in the upper right corner of the figure. The *open triangles* at $\log[L_B/L_{B,\odot}] > 13$ represent data from Fan et al (2001b). The *open squares* are derived from the X-Ray data presented by Barger et al. (2003), who plot the number density of AGN as a function of redshift in the rest frame soft X-Ray (E=0.5-2.0 keV) luminosity range $L_X = 10^{43} - 10^{44}$ ergs s⁻¹ (hereafter, the 'faint bin') and $L_X = 10^{44} - 10^{45}$ ergs s⁻¹ (hereafter, the 'bright bin'). For the Sazonov et al. (2004) template spectrum, the ratio of the rest frame soft X-Ray (denoted by L_X) to blue band luminosity is $L_X/L_B \sim 0.5$. The faint and bright bins of Barger et al. (2003) therefore constitute the range $L_B = 5 \times 10^{10} - 5 \times 10^{11} L_{B,\odot}$ and $L_B = 5 \times 10^{11} - 5 \times 10^{12} L_{B,\odot}$, respectively. To convert the X-Ray number density to the luminosity function, $\Psi(L_B, z)$, we simply divided n_{faint} by the total luminosity width of the bin. We use $n_{\text{faint}} = (1.0^{+3.0}_{-0.8}) \times 10^{-6}$ Mpc⁻³ in both bins.

The error-bars on our constraints reflect the uncertainty in the exact ratio of $L_B/L_{\text{Ly}\alpha}$ (Eq. 4) and denote the 95% confidence levels. Note that upper limits on $\Psi(L_{B,\min}, z)$ as a function of $L_{B,\min}$ have power law slopes of -1 (see Eq. 7). The constraints from the wide field surveys lie on or slightly below the model predictions of Wyithe & Loeb (2003) (shown as the *solid lines*). This implies that the absence of $z = 5.7$ and $z = 6.5$ AGN in wide-field narrow-band surveys rules out this model at $\geq 95\%$ confidence levels at both redshifts, at these low luminosities.

3.2.2 Constraints on $\Psi(L_B, z)$ at $z = 4.5$.

The above constraints at $z > 5$ assumed that $\beta_l = 1.66$. However, as will be discussed below, at $z = 4.5$, extrapolation of this powerlaw from the X-Ray constraint at $\log[L_B/L_{B,\odot}] \sim 11$ to $L_{B,\min}$, would have resulted in a number density of AGN that lies above the implied upper limit. To better constrain the luminosity function, $\Psi(L_{B,\min}, z)$, and its slope at $z = 4.5$, we combine the upper limit on the AGN number density from the Ly α survey with the AGN number densities derived from X-ray data (Barger et al. 2003; Cowie et al. 2003). We use $n_{\text{bright}} = (1.0 \pm 0.5) \times 10^{-6}$ Mpc⁻³ and $n_{\text{faint}} = (3.3 \pm 1.3) \times 10^{-6}$ Mpc⁻³, which we

obtained by interpolating between the $z = 3.5$ and $z = 5.7$ data points of Barger et al. (2003).

We assume the luminosity function, $\Psi(L_B, z)$ to be of the form $kL^{-\beta_l}$. The number density of AGN in the faint X-ray bin, n_{faint} , fixes k as a function of β_l . Extrapolating this luminosity function to lower luminosities, gives us the expected number density of AGN in the Ly α bin, $n_{\text{AGN}} = k \int_{L_{B,\min}}^{L_{B,\max}} dL L^{-\beta_l}$. One of the selection criteria Dawson et al. (2004) use to select $z = 4.5$ Ly α emitter candidates states that a $z = 4.5$ candidate must not be detected in the B_W band of the NOAO deep wide-field survey (Malhotra & Rhoads 2002). We show in § 4.2 that this implies that $L_{B,\max} \sim 2 \times 10^{11} L_{B,\odot}$. For a fixed β_l , we obtain a unique n_{AGN} . Since n_{AGN} is only known as an upper limit, this allows us to put an upper limit on β_l as follows.

In the absence of AGN within the volume probed by the Ly α survey, the probability that the true number was lies between μ and $\mu + d\mu$ is given by $dP = \exp(-\mu)d\mu$ (where we have assumed a Poisson distribution). This may be recast as

$$P(< \mu) = 1 - e^{-\mu}, \quad (8)$$

which gives the probability that the expected number of AGN within the survey volume is less than μ . The expected number of AGN is given by

$$\mu = V_{\text{survey}} \int_{L_{B,\min}}^{L_{B,\max}} dL \Psi(L, z). \quad (9)$$

For a fixed $L_{B,\max}$, we find that μ is a function of $L_{B,\min}$, n_{faint} and β_l only. In the *left panel* of Figure 2 the *thin black solid line* shows the probability $P(< \beta_l)$ as a function of β_l , for the fiducial values of $L_{B,\min} = L_{\text{Ly}\alpha,c}$ and $n_{\text{faint}} = 3.3 \times 10^{-6}$ Mpc⁻³. In this case $P(< 0.60) = 0.95$, i.e. the slope is $\beta_l \lesssim 0.60$ at the 95% confidence level. To illustrate the dependence of $P(< \beta_l)$ on $L_{B,\min}$, and n_{faint} , we have also plotted $P(< \beta_l)$ for $(n_{\text{faint}}, L_{B,\min}) = (2.0 \times 10^{-6} \text{ Mpc}^{-3}, L_{\text{Ly}\alpha,c})$ (*blue dashed line*) and $(3.3 \times 10^{-6} \text{ Mpc}^{-3}, 2.0 L_{\text{Ly}\alpha,c})$ (*red dotted line*). The $2 - \sigma$ upper limit on β_l increases with decreasing n_{faint} and increasing $L_{B,\min}$. To eliminate the dependence of $P(< \beta_l)$ on $L_{B,\min}$ and n_{faint} , we marginalise over these parameters

$$\mathcal{P}_{\text{marg}}(< \beta_l) = \int dn_{\text{faint}} \int dL_{B,\min} \frac{dP}{dn_{\text{faint}}} \frac{dP}{dL_{B,\min}} \times [1 - e^{-\mu(n_{\text{faint}}, L_{B,\min}, \beta_l)}], \quad (10)$$

where dP/dn_{faint} and $dP/dL_{B,\min}$ are the probability distributions for n_{faint} and $L_{B,\min}$, respectively. We choose dP/dn_{faint} to be Gaussian with $n_{\text{faint}} = (3.3 \pm 1.3) \times 10^{-6}$ Mpc⁻³, and $dP/dL_{B,\min}$ to be log normal with $\log(L_{B,\min}/L_{B,\odot}) = 10.2 \pm 0.2$ (this range is motivated by the distribution in the ratio $L_{\text{Ly}\alpha}/L_B$, found from Eq. 4 in § 2). The marginalised constraint is given by the *thick solid line* in Figure 2, which shows that $\beta_l \lesssim 1.0$ at the 95% confidence level. The *right panel* of Figure 2 shows the expected value of $\Psi(L_{B,\min}, z)$ as a function of β_l . The constraint $\beta_l < 1.0$ yields $\log[\Psi(L_{B,\min}, z)] < -7.1$ and is shown as the *filled circle*. This $2 - \sigma$ upper limit on $\Psi(L_{B,\min}, z)$ at $z = 4.5$ is also shown in the left panel of Figure 1 as the *filled circle*. The *open triangles* at $\log[L_B/L_{B,\odot}] > 13$ represent data

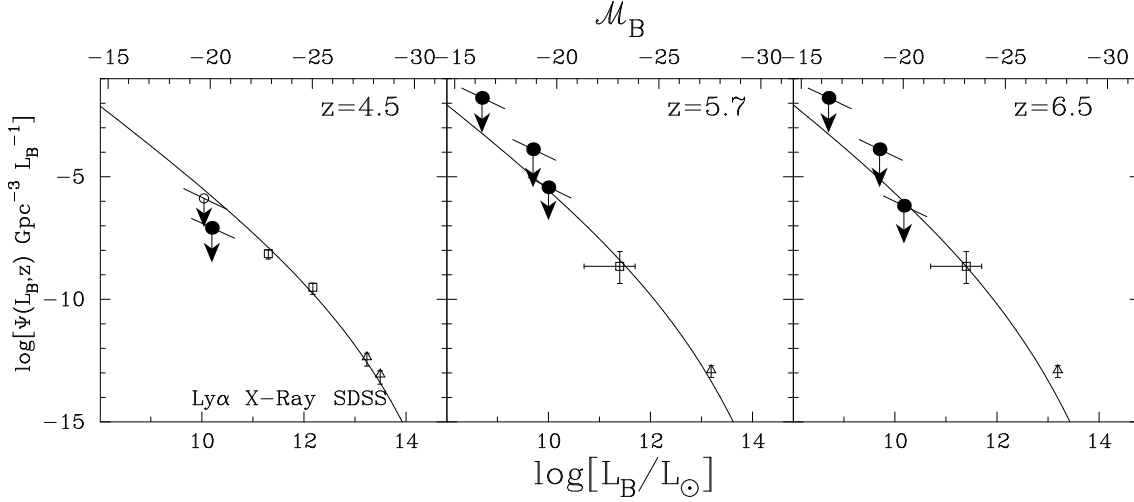


Figure 1. Ly α constraints on the quasar B-band luminosity function, $\Psi(L_B, z)$ at redshifts $z = 4.5$ (left panel), $z = 5.7$ (middle panel) and 6.5 (right panel), plotted as *filled circles* at $\log[L_B/L_{B,\odot}] \lesssim 10$. The error-bars on the Ly α constraints denote 95% confidence limits. The *open circle* at $z = 4.5$ denotes the upper limit obtained from spectroscopic data alone (§ 3.3). The SDSS and X-Ray data are taken from Fan et al (2001,2001b) (*open triangles*) and Barger et al. (2003) (*open squares*), respectively. This figure shows that: 1) existing Ly α surveys allow the quasar B-band luminosity function to be constrained at B-band luminosities as low as $\log[L_B/L_{B,\odot}] = 8.5$ (or at absolute magnitude $M_B \sim -16$); and 2) the absence of AGN in existing Ly α surveys at $z = 4.5$ suggests that the quasar luminosity function at $z = 4.5$ is increasing more slowly towards lower luminosities than the model predictions of Wyithe & Loeb (2003) (shown as the *solid lines*). In fact, $\partial \log \Psi / \partial \log L_B \geq -1.0$ (95% confidence level) for $\log[L_B/L_{B,\odot}] \lesssim 11$ (also see Fig. 2).

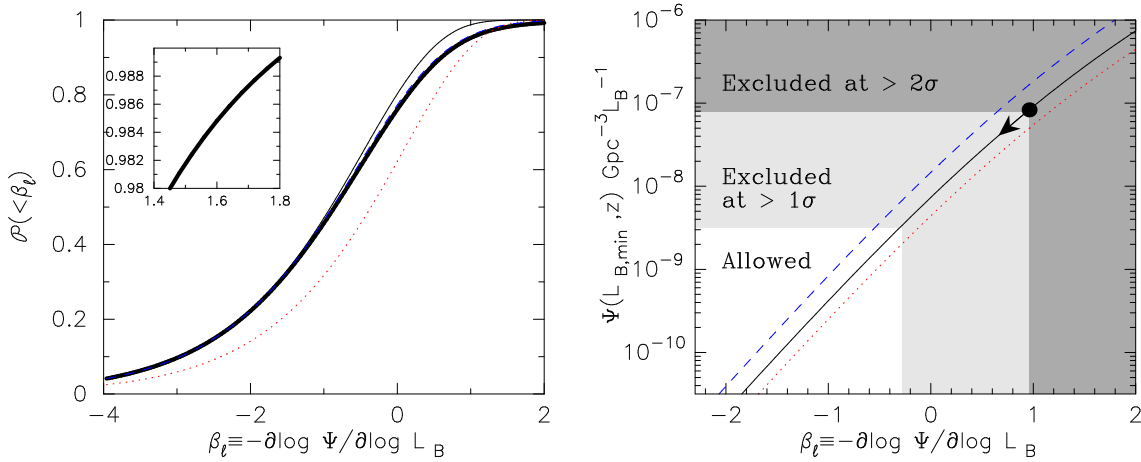


Figure 2. *Left Panel:* The probability $P(< \beta_l)$ that $-\partial \log \Psi / \partial \log L_B$ is less than β_l . The *thin black solid line* represents the constraint for the fiducial model with $L_{B,\min} = L_{\text{Ly}\alpha,c}$ and $n_{\text{faint}} = 3.3 \times 10^{-6} \text{ Mpc}^{-3}$, for which $P(< 0.6) = 0.95$. The effect of lowering n_{faint} (*red dotted line*, $n_{\text{faint}} = 2.0 \times 10^{-6} \text{ Mpc}^{-3}$) and increasing $L_{B,\min}$ (*blue dashed line*, $L_{B,\min} = 2.0 L_{\text{Ly}\alpha,c}$) is to reduce $P(< \beta_l)$. The opposite is true when $L_{B,\min}$ is decreased and n_{faint} is increased. The *thick solid line* shows the probability, $\mathcal{P}_{\text{marg}}(< \beta_l)$, after marginalizing over $L_{B,\min}$ and n_{faint} . The inset shows that $\mathcal{P}_{\text{marg}}(< 1.6) = 0.99$, i.e. $\partial \log \Psi / \partial \log L_B > -1.6$ at the 99% confidence level. We find marginal evidence (76% confidence level) that, in fact, the luminosity function falls towards lower luminosities ($\mathcal{P}_{\text{marg}}(< 0.0) = 0.76$) below $\log[L_B/L_{B,\odot}] = 11$. *Right Panel:* The expected value of $\Psi(L_{B,\min}, z)$ is plotted as a function of β_l for the models shown in the left panel. The marginalised $2 - \sigma$ upper limit is shown as the *large filled circle*, which implies $\log[\Psi(L_{B,\min}, z)] < -7.1$. This constraint is also shown in Figure 1. The light and dark grey areas demarcate the region of (β_l, Ψ) -space excluded at the $> 68\%$ ($1 - \sigma$) and $> 95\%$ ($2 - \sigma$) confidence level, after marginalising over n_{faint} and $L_{B,\min}$. For reference, the model of Wyithe & Loeb (2003) predicts $\log \Psi \sim -5.7$.

from Fan et al (2001) and the *open squares* represent the X-ray constraints derived from the data presented by Barger et al. (2003) and Cowie et al. (2003). Figure 1 implies that at $z = 4.5$, the QLF flattens below $\log(L_B/L_{B,\odot}) \sim 11$, as may also be seen via the model quasar luminosity function from Wyithe & Loeb 2002 and 2003 (plotted as the *black solid line* in Fig. 1). It is worth pointing out how the ex-

act marginalised constraint on β_l depends on the assumed survey sensitivity. If we decrease/increase f_{lim} by a factor of 2 then $\beta_l < 0.8/1.4$ at the 95% confidence level, respectively. The value of $\mathcal{P}_{\text{marg}}(< 0.0)$ barely depends on f_{min} . The decreased sensitivity corresponds approximately to the sensitivity limit reported by Dawson et al. (2004), while the

increased sensitivity corresponds to the sensitivity derived from their actual faintest Ly α detections.

The constraints obtained so far only used the non-detection of broad line emitters in the narrow band survey. Dawson et al. (2004) also obtained spectra of 25 of their candidate LAEs. Below, we constrain $\Psi(L_B, z)$ using this spectroscopic data.

3.3 Constraints on $\Psi(L_B, z)$ at $z = 4.5$ from Spectroscopic Follow-Up.

Dawson et al. (2004) obtained follow-up high resolution spectra for 25 candidate LAEs. Of these 25 candidates, 18 were genuine $z = 4.5$ objects and the other 7 were either not detected (6) or a lower redshift [O II] emitter (1). All 18 $z = 4.5$ objects were identified as galaxies, based on 1) the observed narrow physical line widths of the Ly α lines ($\Delta v \lesssim 500 \text{ km s}^{-1}$, also see § 4.1), and 2) the lack high-ionization state UV emission lines, symptomatic of AGN activity, in their spectra. If the sample of 350 detections contains less than 10% AGN, $f_{\text{AGN}} \lesssim 0.1$, then the probability that a random sample of 25 contains no AGN is $\sim (1 - f_{\text{AGN}})^{25} \gtrsim 0.05$ (In § 4.3 we show that $f_{\text{AGN}} \lesssim 0.1$ is consistent with the constraints imposed by the X-Ray observations of Wang et al. 2004). From the spectroscopic data alone, we can therefore put a $2 - \sigma$ upper limit on the number of AGN within the original survey volume ($1.5 \times 10^6 \text{ Mpc}^3$) at $N_{\text{AGN}} \lesssim 350 f_{\text{AGN}} = 35$ down to a Ly α flux of $1.1 \times 10^{-17} \text{ ergs s}^{-1} \text{ cm}^{-2}$. Using Eq (7) we obtain an upper limit on $\Psi(L_B, z)$, which is shown as the *open circle* in Figure 1. This constraint on $\Psi(L_B, z)$ is weaker than our original constraint, but still rules out the model luminosity function at $> 95\%$.

4 THE NATURE OF VERY FAINT AGN AND THEIR OBSERVABLE PROPERTIES.

We have demonstrated how Ly α surveys may be used to constrain the (very) faint end of the quasar luminosity function. This constraint is purely empirical and we stress that so far no details of the process of gas accretion onto black holes have been assumed. The following discussion focuses on the nature of faint AGN (with $\log[L_B/L_{B,\odot}] \lesssim 10$). First, we present a more general calculation of the observable Ly α properties of AGN. The result of this calculation allows us to determine the range of black hole masses probed by Ly α surveys and may be used to identify AGN among known Ly α emitters, especially in combination with our estimates for the observable properties of these faint AGN in the optical (§ 4.2) and X-ray (§ 4.3) bands.

4.1 Observable Ly α Properties of Faint AGN

First we discuss the intrinsic Ly α properties of AGN. The Kaspi relation (Kaspi et al. 2000; Peterson et al. 2004) relates the mass of the black hole powering the quasar, M_{BH} , to its continuum luminosity at 5100 Å

$$M_{\text{BH}} = 7.6 \pm 1.3 \times 10^7 \left(\frac{\lambda F_\lambda(5100\text{\AA})}{10^{44} \text{ erg s}^{-1}} \right)^{0.79} M_\odot. \quad (11)$$

We define the ratio $\mathcal{R} \equiv [\lambda F_\lambda(1200 \text{ \AA})]/[\lambda F_\lambda(5100 \text{ \AA})] = [EF_E(1200 \text{ \AA})]/[EF_E(5100 \text{ \AA})]$ (see § 2). The template given by Sazonov et al. (2004) yields $\mathcal{R} = 1.8$. For a given Ly α EW, the Ly α luminosity is therefore uniquely determined by M_{BH} through

$$L_{\text{Ly}\alpha,43} = 2.3 \left(\frac{\text{EW}}{140\text{\AA}} \right) \left(\frac{M_{\text{BH}}}{7.6 \times 10^7 M_\odot} \right)^{1.3}, \quad (12)$$

where $L_{\text{Ly}\alpha,43}$ is in units of $10^{43} \text{ ergs s}^{-1}$. The Ly α emission lines from AGN are broader than those of galaxies. Kaspi et al. (2000) and Peterson et al. (2004) found the Half Width at Half Maximum (HWHM) of the Balmer lines to be related to the continuum luminosity at 5100 Å. If the same relation holds for the Ly α line, then its HWHM is given by

$$v_{\text{HWHM}} = 2 \times 10^3 \left(\frac{M_{\text{BH}}}{7.6 \times 10^7 M_\odot} \right)^{-0.34} \text{ km s}^{-1}. \quad (13)$$

Note that the observations presented in Kaspi et al. (2000) (their Figure 7) suggest that v_{HWHM} does not increase beyond $v_{\text{HWHM}} \sim 3 \times 10^3 \text{ km s}^{-1}$ at low masses.

To obtain the AGNs' observed properties in the Ly α line from the above relations, we require knowledge of the fraction of transmitted Ly α -flux through the IGM as a function of frequency. We first focus on the observed Ly α properties of AGN at $z = 4.5$ and $z = 5.7$. Although the universe is fully reionised at $z < 6$ (e.g. Fan et al. 2002), a trace quantity of neutral hydrogen is sufficient to scatter Ly α blueward of the Ly α line center out of our line of sight. For this reason the IGM, to first order, erases the blue half of the Ly α line, so that the IGM transmission is $\mathcal{T} = 0.5$. Various refinements of this scenario are possible. Infall of the IGM around massive objects causes the IGM to erase a part of the red side of the Ly α line as well (Barkana 2004), which reduces \mathcal{T} . On the other hand, the proximity effect around these fainter AGN increases \mathcal{T} . These two effects counteract each other, and ignoring both does not add a significant error to our estimate of \mathcal{T} . This is especially true when considering the large width of the Ly α line emitted by AGN. When the IGM erases the blue half of the Ly α line, the observed v_{HWHM} is reduced by a factor of 2 relative to the value in Eq (13). Note that $v_{\text{HWHM}} = 1500 \text{ km s}^{-1}$ corresponds to an observed FWHM of $(1+z)2v_{\text{HWHM}}/c \sim 66\text{\AA}$ at $z = 4.5$ (this value was used in § 3.1).

At $z = 6.5$, the IGM is believed to contain a significant fraction of neutral hydrogen (Wyithe & Loeb 2004; Mesinger & Haiman 2004; Fan et al. 2005). For Ly α sources embedded in a neutral IGM, the damping wing of the Gunn-Peterson trough can extend to the red side of the line and erase a significant fraction of the total Ly α flux. However, this effect is reduced when the Ly α source is surrounded by an HII region (Cen & Haiman 2000; Madau & Rees 2000). Moreover, sources with sufficiently broad emission lines ($v_{\text{HWHM}} > 300 \text{ km s}^{-1}$) can remain detectable even in the absence of such an HII region (Haiman 2002). In Appendix A we show that a representative number for the IGM transmission \mathcal{T} for faint AGN embedded in a neutral IGM at $z = 6.5$ is $\mathcal{T} = 0.3$ and that the observed v_{HWHM} is reduced, again by a factor of ~ 2 relative to the value in Eq (13). Furthermore, we show that the Gunn Peterson damping wing may cause the observed line center of AGN at $z = 6.5$ to be redshifted by up to $\sim 2000 \text{ km s}^{-1}$ relative to other emission lines (see Appendix A).

Next, we write the total detectable Ly α flux of AGN as

$$\begin{aligned} f_{\alpha} &= \frac{L_{\alpha}}{4\pi d_L^2(z)} \mathcal{T} \\ &\approx 5 \times 10^{-17} \left(\frac{M_{\text{BH}}}{7.6 \times 10^7} \right)^{1.3} \\ &\times \left(\frac{\mathcal{T}}{0.5} \right) \left(\frac{\text{EW}}{140 \text{ \AA}} \right) \left(\frac{1+z}{6} \right)^{-2.8} \text{ erg s}^{-1} \text{ cm}^{-2} \end{aligned} \quad (14)$$

in which $\mathcal{T} \sim 0.5$ for $z < 6$ and $\mathcal{T} \sim 0.3$ for $z = 6.5$. To allow f_{α} to be written as a simple function of $(1+z)$, we approximated the luminosity distance by $d_L(z) = 3.6 \times 10^4 ([1+z]/5)^{1.4}$ Mpc, which is within $< 6\%$ of its actual value in the range $z = 3 - 10$. Eq (14) shows that existing Ly α surveys could have detected AGN powered by black holes with masses of $M_{\text{BH}} \sim 10^6 - 10^7 M_{\odot}$ at $z = 4.5 - 6.5$.

Equation (14) assumed that the Kaspi-relations derived from observations of luminous AGN also relate the black-hole mass to the Ly α luminosity for low luminosity AGN. Alternatively, if we assume that faint AGN are powered by less massive black holes accreting at their Eddington limit, then these black-holes are up to ~ 5 orders of magnitude less massive than those of the observed SDSS quasars, yielding $M_{\text{BH}} \sim$ a few $10^4 M_{\odot}$. Combined with the above argument, we therefore conclude that existing Ly α surveys could have detected AGN powered by black holes with masses in the range $M_{\text{BH}} = 10^4 - 10^7 M_{\odot}$ at $z = 4.5 - 6.5$. Here, the lower end of this mass range is probed only by the spectroscopic surveys of gravitationally lensed regions.

4.2 AB-magnitudes of Faint AGN

Using the template spectrum for AGN given by Sazonov et al. (2004), we calculate the apparent AB-magnitude of faint AGN as a function of observed wavelength. The AB-magnitude of an object with flux density F_{ν} (in ergs s $^{-1}$ cm $^{-2}$ Hz $^{-1}$) is

$$m_{AB} = -48.6 - 2.5 \log(F_{\nu}). \quad (15)$$

At rest frame energies $E < 10$ eV and $E > 10$ eV, the AGN continuum follows the power-laws $F_{\nu} \propto \nu^{-0.6}$ and $F_{\nu} \propto \nu^{-1.7}$, respectively (Sazonov et al. 2004). For an AGN whose Ly α flux is $f_{\alpha,17} \times 10^{-17}$ ergs s $^{-1}$ cm $^{-2}$, the apparent magnitude may then be written as

$$m_{AB}(\lambda) = 26.8 - 2.5 \left[\log \left(\frac{5.5}{1+z} \right) + \log \mathcal{K}(\lambda) \right],$$

where

$$\begin{aligned} \mathcal{K}(\lambda) &= \left(\frac{f_{\alpha,17}}{2} \right) \left(\frac{140 \text{ \AA}}{\text{EW}} \right) \left(\frac{0.5}{\mathcal{T}} \right) \left(\frac{\lambda}{\lambda_{\alpha,z}} \right)^{0.6} \quad \lambda > \lambda_{\alpha,z}, \\ &= \langle e^{-\tau} \rangle \left(\frac{f_{\alpha,17}}{2} \right) \left(\frac{140 \text{ \AA}}{\text{EW}} \right) \left(\frac{0.5}{\mathcal{T}} \right) \left(\frac{\lambda}{\lambda_{\alpha,z}} \right)^{1.7} \quad \lambda < \lambda_{\alpha,z}. \end{aligned} \quad (16)$$

Here $\lambda_{\alpha,z}$ is the redshifted Ly α wavelength ($\lambda_{\alpha,z} = 1216[1+z]$ \AA).

In Figure 3 we plot m_{AB} as a function of observed wavelength, λ in the range $\lambda = 2000 - 10000$ \AA for three values of the total flux in the Ly α line, $f_{\alpha,17} = 20$ (*black solid line*), 2 (*red dashed line*) and 0.4 (*blue dotted line*), all at $z = 4.5$. We assumed the Ly α equivalent width to be EW = 140 \AA. The break at $\lambda = 6700$ \AA is the Lyman break caused by the IGM; the Ly α forest reduces the mean flux blueward of the

Ly α line by a factor of $\langle e^{-\tau} \rangle$. This factor has been determined observationally and is $\langle e^{-\tau} \rangle = 0.25$ at $z = 4.5$ (e.g. Fan et al. 2002). Figure 3 (and Eq. 18) shows that AGN with $f_{\alpha} \gtrsim f_{\text{max}} = 2 \times 10^{-16}$ ergs s $^{-1}$ cm $^{-2}$ have a B_W apparent magnitude of $m_{AB} \lesssim 26.6$ ($\lambda \sim 4400$ \AA). These AGN would have been detected at the $\gtrsim 5 - \sigma$ level in the B_W band of the NOAO deep wide-field survey (Jannuzi & Dey 1999, this detection limit is indicated by the *thick horizontal line* at $m_{AB} = 26.6$). Since one of the selection criteria Dawson et al. (2004) use to select $z = 4.5$ Ly α emitter candidates states that a $z = 4.5$ candidate must not be detected in the B_W band of the NOAO deep wide-field survey (Malhotra & Rhoads 2002), AGN with $f_{\alpha} \gtrsim f_{\text{max}} = 2 \times 10^{-16}$ ergs s $^{-1}$ cm $^{-2}$ would not have made it into the sample. Therefore, with the current selection criteria, the Ly α survey performed by Dawson et al. (2004) only probes AGN in the luminosity range $L_B \in [L_{B,\text{min}}, L_{B,\text{max}}]$, with $L_{B,\text{max}} \sim 2 \times 10^{11} L_{B,\odot}$ (this luminosity was used in § 3.2.2).

4.3 X-Ray Emission from Faint AGN

X-Rays provide a reliable pointer to AGN activity. Using the Sazonov et al. (2004) template, we calculate the ratio of detectable Ly α and X-Ray flux (in the observed 0.5-10.0 keV band)

$$\frac{f_{\alpha}}{f_X} \sim 0.07 \left(\frac{\mathcal{T}}{0.5} \right) \left(\frac{\text{EW}}{140 \text{ \AA}} \right). \quad (17)$$

This ratio changes by less than $\sim 10\%$ between $z = 4.5 - 6.5$. The total X-Ray flux in the observers' 0.5-10.0 keV band is ~ 14 times higher than the total Ly α flux. For example, an AGN with a detected Ly α flux of 2×10^{-17} ergs s $^{-1}$ cm $^{-2}$ is expected to have an X-ray flux of $\sim 3 \times 10^{-16}$ ergs s $^{-1}$ cm $^{-2}$. This lies slightly below the quoted $3 - \sigma$ detection limit in the X-ray observations of individual Ly α emitter candidates presented by Wang et al. (2004) ($\sim 6.6 \times 10^{-16}$ ergs s $^{-1}$ cm $^{-2}$ in the 0.5-10.0 keV band). Therefore, even if AGN were in the sample, these X-ray observations would not necessarily have revealed them (§ 3.1). Also, provided the fraction of AGN is $f_{\text{AGN}} \lesssim 0.1$ (§ 3.3), these would not have appeared in the stacked X-ray image, since stacking 101 images increases the noise by $101^{1/2}$, whereas the X-Ray signal from AGN would increase by $f_{\text{AGN}} \times 100 \lesssim 10$. The signal-to-noise ratio would thus be conserved at best.

Similarly, the total X-Ray flux in the observers' 0.5-2.0 keV band is ~ 4 times higher than the total Ly α flux. It may come as a surprise then, that our constraints are fainter than those inferred from the *Chandra Deep Field*. The X-Ray detection threshold in the *Chandra Deep Field North* in the 0.5-2.0 keV band is $\sim 1.5 \times 10^{-17}$ ergs s $^{-1}$ cm $^{-2}$, which would correspond to a Ly α flux of $\sim 4 \times 10^{-18}$ ergs s $^{-1}$ cm $^{-2}$, well below the sensitivity limit of $f_{\text{lim}} \sim 1.1 \times 10^{-17}$ ergs s $^{-1}$ cm $^{-2}$ in the survey performed by Dawson et al. (2004). However, estimates of the photometric redshifts for the X-Ray sources require that they be bright enough to be detected in the Subaru Sloan z' band (which is centered on $\lambda \sim 9000$ \AA). This imposes a flux limit corresponding to AB magnitudes of the X-Ray sources in the Sloan z' band that are below $\lesssim 25.2$. Using the quasar template, we find that this excludes AGN with B-Band luminosities less than $6 \times 10^{10} L_{B,\odot}$, which agrees very well with the lower luminosity bound of the 'faint' X-ray bin in § 3.2.2.

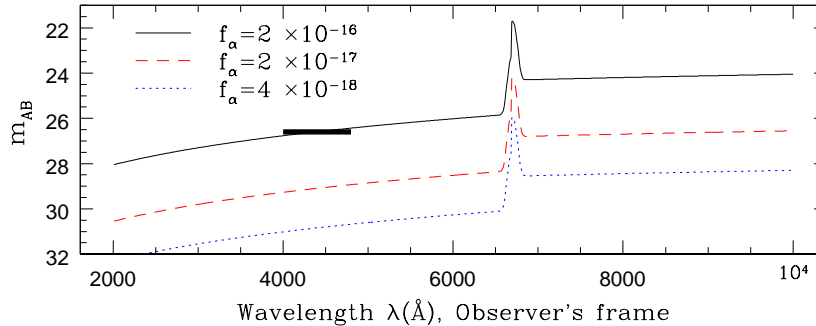


Figure 3. Model spectra of faint AGN at $z = 4.5$ with observable Ly α flux, $f_\alpha = 2 \times 10^{-16}$ (black solid line), 2×10^{-17} (red dashed line) and 4×10^{-18} (blue dotted line) $\text{ergs s}^{-1} \text{cm}^{-2}$. The template spectrum of Sazonov et al. (2004) was normalised to produce the correct Ly α flux (see Eq. 16). For this plot, the AGN’s rest frame Ly α equivalent width was assumed to be $\text{EW}=140 \text{ \AA}$. The break at $\lambda = 6700 \text{ \AA}$ is the Lyman break caused by the IGM (see § 4.2). This figure shows that: 1) AGN with $f_\alpha \gtrsim 2 \times 10^{-16} \text{ ergs s}^{-1} \text{cm}^{-2}$ have a B_W apparent magnitude of $m_{AB} \lesssim 26.6$. These AGN would have been detected in the NOAO deep field (whose detection limit is indicated by the *thick horizontal line* at $m_{AB} = 26.6$) and would therefore have been discarded as being candidate high redshift Ly α emitters (Malhotra & Rhoads 2002). Furthermore, the figure shows that AGN with $f_\alpha = 4 \times 10^{-18} \text{ ergs s}^{-1} \text{cm}^{-2}$, which corresponds to Taniguchi et al. (2005)’s detection limit, have apparent magnitudes $m_{AB} \gtrsim 28$, which makes them difficult to detect at other wavelengths.

The previous discussion demonstrates an observational bias against identification of high redshift faint AGN in deep X-Ray observations. Within narrow redshift windows, this bias could be alleviated by combining X-Ray observations with deep Ly α observations, since the detection of a Ly α line would determine the AGN’s redshift. Similarly, the bias against identifying bright AGN in wide field Ly α surveys (§ 4.2) could be alleviated in combination with deep X-ray observations. These points illustrate the utility of combining deep X-Ray and Ly α observations to identify faint AGN, provided the sensitivities in each observation probe the same population of AGN.

5 DISCUSSION

We have shown that at $z = 4.5$ and below $M_B \sim -20$, the quasar B-band luminosity function rises more slowly towards lower luminosities, $\partial \log \Psi / \partial \log L_B \gtrsim -1.0$ (95% confidence level), than has been observed at higher luminosities and lower redshifts, where $\partial \log \Psi / \partial \log L_B \sim -1.6$ (Pei 1995; Boyle et al. 2000). This flattening of the faint end of the luminosity function towards higher redshift is consistent with the recent work by Hunt et al. (2004), who found that $\partial \log \Psi / \partial \log L_B = -1.24 \pm 0.07$ at $z = 3$. We find marginal evidence (76% confidence level) that, in fact, the luminosity function falls towards lower luminosities below $M_B \sim -20$. This finding is in contrast to observations at higher luminosities. Moreover the observed number counts lie well below the model predictions of Wyithe & Loeb 2003 (Fig. 1). This may be explained in three ways:

1) Our work has focused on the luminosity function of broad-lined AGN (Type I), which in the unified model for AGN are the same as Type II AGN (e.g. Norman et al. 2002), but unobscured by the thick absorbing torus. Simpson (2005) has shown that the fraction of type I AGN decreases with luminosity, which is supported theoretically by

the ‘receding torus’ model (e.g. Lawrence 1991). This would imply that a luminosity function that incorporates both type I and II AGN does not flatten as much at $z = 4.5$ as shown in Figure 1. However, to fully explain the observed flattening of the luminosity function requires the fraction of type I AGN to decrease by $\sim 1 - 2$ orders of magnitude between $\log[L_B/L_{B,\odot}] = 10$ and ~ 11.5 . Since this luminosity dependence of the type I AGN fraction is much stronger than has been observed, this is very unlikely.

2) Gas accretion onto black holes in the mass-range $M_{\text{BH}} = 10^6 - 10^7 M_\odot$ is suppressed. One origin of this suppression may be negative AGN feedback. AGN with $\log[L_B/L_{B,\odot}] = 10.5$ are typically powered by black holes in the mass range $M_{\text{BH}} \sim 10^6 M_\odot$ to a few $10^7 M_\odot$ (§ 4.1). According to the relation between M_{BH} and the circular velocity v_{circ} of the dark matter halo that hosts the black hole [Ferrarese & Merritt (2000); Ferrarese (2002)], this corresponds to $v_{\text{circ}} = 100 - 250 \text{ km s}^{-1}$. For comparison, suppression of accretion due to a photoionised IGM at $z = 4.5 - 6.5$ only occurs at $v_{\text{circ}} = 40 - 60 \text{ km s}^{-1}$ (e.g. Dijkstra et al. 2004). However, Dekel & Silk (1986) have shown that supernova driven gas loss as a result of the first burst of star formation becomes significant in halos with $v_{\text{circ}} \lesssim 100 \text{ km s}^{-1}$. The latter feedback mechanism would therefore provide a more plausible explanation for the reduced gas accretion efficiency onto black holes in the mass range $M_{\text{BH}} \sim 10^6 M_\odot - \text{a few } 10^7 M_\odot$.

3) The number of black holes in the range $M_{\text{BH}} = 10^5 - 10^7 M_\odot$ is lower than expected from the $M_{\text{BH}} - v_{\text{circ}}$ relation by \sim two orders of magnitude. Haiman et al. (2004) used the rareness of black holes with masses $M_{\text{BH}} \lesssim 10^7 M_\odot$ as a possible explanation for their model of the luminosity function of radioloud quasars to overpredict the abundance of faint radio sources, by one-two orders of magnitude. The possible reduction in the number of black holes with masses $M_{\text{BH}} \lesssim 10^7 M_\odot$, may reflect the existence of a minimum super massive black hole mass, as envisioned in some formation

scenarios (e.g. Haehnelt et al. 1998, in which the minimum black hole mass would be $M_{\text{BH}} = 10^6 M_{\odot}$).

Our finding that at $z = 4.5$ the QLF flattens more than previously believed for $\log[L_B/L_{B,\odot}] \lesssim 11$ also implies that faint AGN contribute less photons to the ionising background than previously thought. However, this is only a small effect since the total ionising photon output from AGN per unit volume is $\propto \int L\Psi(L, z)dL \propto \int L^{-\beta_i+1}dL$. For $\beta_i < 2$, this integral is dominated by luminous AGN. A more intriguing implication concerns miniquasars, which are quasars powered by black holes in the mass range $M_{\text{BH}} = 10 - 10^5 M_{\odot}$. It has been suggested that miniquasars could contribute significantly to the ionising background at high redshift (Madau et al. 2004; Ricotti & Ostriker 2004). However, if quasar activity decreases with decreasing black hole mass (as our results suggest), and if this trend continues into the miniquasar-realm, then it follows that miniquasars would not be efficient producers of ionizing radiation and would not have contributed significantly to the ionizing background. It is worth emphasising that this miniquasar-realm may be accessible with existing deep spectroscopic surveys of gravitationally lensed regions (Santos et al. 2004). In these surveys, black holes with masses of $M_{\text{BH}} \sim 10^4 M_{\text{BH}}$ can be detected, provided these are accreting at their Eddington limit (§ 4.1). Currently, the only observational constraints on the abundance of high redshift miniquasars are derived from the cosmic X-Ray and infrared backgrounds (Dijkstra et al. 2004b, Salvaterra et al. 2005).

6 CONCLUSIONS

Recent Ly α surveys have detected Ly α emitting objects from redshifts as high as $z = 6.5$, and at luminosities as low as $10^{41} \text{ erg s}^{-1}$ (e.g. Santos et al. 2004). No evidence of AGN activity exists among these several hundred Ly α emitters (Dawson et al. 2004; Wang et al. 2004; Taniguchi et al. 2005). Wide field Ly α surveys are designed to deeply image wide fields on the sky, yielding survey volumes in a narrow shell of redshift space as large as $10^5 - 10^6 \text{ Mpc}^3$, while deep spectroscopic surveys of gravitationally lensed regions probe deeper into smaller volumes. The absence of AGN within these fields places a tight upper limit on the number density of AGN with Ly α luminosities exceeding the surveys detection thresholds, $L_{\text{Ly}\alpha, c}$.

In § 2 we have shown empirically that the Ly α luminosities of AGN equal their B-band luminosities to within a factor of a few (Eq. 4). As a result, deep Ly α surveys can be used to obtain upper limits on the number density of AGN with B-Band luminosities exceeding $L_{B, \text{min}} \sim L_{\text{Ly}\alpha, c}$. When expressed in B-band solar luminosities, $L_{B, \text{min}}$ is $\sim 10^{8.5} L_{B, \odot}$ (which corresponds to an absolute magnitude of $M_B = -16$). In § 4.1 we demonstrated that such AGN are expected to be powered by black holes with masses in the range $M_{\text{BH}} = 10^4 - 10^7 M_{\odot}$ at $z = 4.5 - 6.5$.

We derive upper limits on AGN number densities and constrain the quasar B-band luminosity function $\Psi(L_{B, \text{min}}, z)$ at a luminosity $L_{B, \text{min}}$. The non-detection of AGN among $z = 4.5 - 6.5$ LAEs rules out the model predictions by Wyithe & Loeb (2003), which successfully reproduce the brighter end of the observed quasar luminosity function at $z = 2 - 6$, at $> 95\%$ confidence levels at all redshifts. At

$z = 4.5$, we find that $\partial \log \Psi / \partial \log L_B \geq -1.6$, the value observed at lower redshifts, for $\log[L_B/L_{B, \odot}] \lesssim 11$ at the 99% confidence level (Fig 2). We find marginal evidence that at these luminosities, the luminosity function rises with luminosity, corresponding to a powerlaw slope > 0 (76% confidence level). In other words, the QLF may increase with L_B at these faint luminosities, in contrast to observations of more luminous AGN. These results represent the faintest observational constraints on the quasar luminosity function at these redshifts to date.

We have found that models of the quasar luminosity function which are successful in reproducing the bright end of the quasar luminosity function predict more AGN to be present than are observed, by up to two orders of magnitude (Fig. 1) at $z \sim 4.5$. These results imply either that accretion onto lower mass black holes is less efficient than onto their more massive counterparts, or that the number of black holes powering AGN with $M_B \gtrsim -20$ is lower than expected from the $M_{\text{BH}} - \sigma$ relation by one-two orders of magnitude. Extrapolating from reverberation-mapping studies suggests that these black holes would have $M_{\text{BH}} = 10^6 - 10^7 M_{\odot}$.

Our work has demonstrated the effectiveness of Ly α surveys in constraining the faint end of the quasar B-band luminosity function. Deeper and larger surveys will allow for a better determination of its slope, and whether indeed the quasar luminosity function rises with luminosity for $M_B \gtrsim -20$ at $z = 4.5$, and at other redshifts. These constraints will offer new insights on the growth of low mass black holes and their relation to the known super massive black holes. To help identify AGN among observed Ly α emitters, we have modeled the observable properties of the Ly α line for high redshift, faint AGN. Using the empirical Kaspi-relations, we estimate that the observable Ly α line widths (Half Width at Half Maximum) of faint AGN will be $\sim 1500 \text{ km s}^{-1}$. For AGN embedded in a neutral medium the peak of the Ly α line is redshifted up to 2000 km s^{-1} relative to the true line center (§ 4.1). To facilitate the identification of these faint AGN, we have estimated their observable properties in the visible (§ 4.2, Fig 3) and X-Ray bands (§ 4.3). We caution that selection criteria used in Ly α surveys to select candidate high redshift Ly α emitters currently introduce a bias against detecting AGN with $\log[L_B/L_{B, \odot}] \gtrsim 11.3$ (§ 4.2), corresponding to the faintest AGN identified in the Chandra Deep Fields.

Acknowledgments Our research is supported by the Australian Research Council. The authors would like to thank Colin Norman for helpful discussions and Zoltán Haiman for useful comments on an earlier version of the manuscript.

REFERENCES

- Barger A. J., Cowie L. L., Capak P., Alexander D. M., Bauer F. E., Brandt W. N., Garmire G. P., Hornschemeier A. E., 2003, ApJL, 584, L61
- Barkana R., 2004, MNRAS, 347, 59
- Boyle B. J., Shanks T., Croom S. M., Smith R. J., Miller L., Loaring N., Heymans C., 2000, MNRAS, 317, 1014
- Cen R., Haiman Z., 2000, ApJL, 542, L75
- Charlot S., Fall S. M., 1993, ApJ, 415, 580

Cowie, L. L., Barger, A. J., Bautz, M. W., Brandt, W. N., & Garmire, G. P. 2003, *ApJL*, 584, L57

Croom S. M., Smith R. J., Boyle B. J., Shanks T., Miller L., Outram P. J., Loaring N. S., 2004, *MNRAS*, 349, 1397

Dawson S., Rhoads J. E., Malhotra S., Stern D., Dey A., Spinrad H., Jannuzi B. T., Wang J., Landes E., 2004, *ApJ*, 617, 707

Dekel, A., & Silk, J. 1986, *ApJ*, 303, 39

Dijkstra M., Haiman Z., Rees M. J., Weinberg D. H., 2004, *ApJ*, 601, 666

Dijkstra, M., Haiman, Z., & Loeb, A. 2004b, *ApJ*, 613, 646

Ellis, R., Santos, M. R., Kneib, J.-P., & Kuijken, K. 2001, *ApJL*, 560, L119

Fan, X., et al. 2001, *AJ*, 121, 54

Fan, X., et al. 2001b, *AJ*, 122, 2833

Fan X., Narayanan V. K., Strauss M. A., White R. L., Becker R. H., Pentericci L., Rix H.-W., 2002, *AJ*, 123, 1247

Fan, X., et al. 2005, *AJ* in press, arXiv:astro-ph/0512082

Ferrarese L., Merritt D., 2000, *ApJL*, 539, L9

Ferrarese L., 2002, *ApJ*, 578, 90

Gunn J. E., Peterson B. A., 1965, *ApJ*, 142, 1633

Haehnelt, M. G., Natarajan, P., & Rees, M. J. 1998, *MNRAS*, 300, 817

Haiman Z., Loeb A., 1998, *ApJ*, 503, 505

Haiman Z., 2002, *ApJL*, 576, L1

Haiman Z., Cen R., 2002, *ApJ*, 578, 702

Haiman, Z., Quataert, E., & Bower, G. C. 2004, *ApJ*, 612, 698

Hasinger, G., Miyaji, T., & Schmidt, M. 2005, *A&A*, 441, 417

Hunt, M. P., Steidel, C. C., Adelberger, K. L., & Shapley, A. E. 2004, *ApJ*, 605, 625

Jannuzi, B. T., & Dey, A. 1999, *ASP Conf. Ser.* 191: Photometric Redshifts and the Detection of High Redshift Galaxies, 191, 111

Kaspi S., Smith P. S., Netzer H., Maoz D., Jannuzi B. T., Givon U., 2000, *ApJ*, 533, 631

Lawrence, A. 1991, *MNRAS*, 252, 586

Madau P., Rees M. J., 2000, *ApJL*, 542, L69

Madau P., Rees M. J., Volonteri M., Haardt F., Oh S. P., 2004, *ApJ*, 604, 484

Malhotra S., Rhoads J. E., 2002, *ApJL*, 565, L71

Malhotra, S., Wang, J. X., Rhoads, J. E., Heckman, T. M., & Norman, C. A. 2003, *ApJL*, 585, L25

Mesinger A., Haiman Z., 2004, *ApJL*, 611, L69

Norman, C., et al. 2002, *ApJ*, 571, 218

Ouchi M., et al. 2005, *ApJL*, 620, L1

Pei, Y. C. 1995, *ApJ*, 438, 623

Peterson, B. M., et al. 2004, *ApJ*, 613, 682

Rhoads J. E., Malhotra S., Dey A., Stern D., Spinrad H., Jannuzi B. T., 2000, *ApJL*, 545, L85

Ricotti M., Ostriker J. P., 2004, *MNRAS*, 352, 547

Salvaterra, R., Haardt, F., & Ferrara, A. 2005, *MNRAS*, 362, L50

Santos, M. R., Ellis, R. S., Kneib, J.-P., Richard, J., & Kuijken, K. 2004, *ApJ*, 606, 683

Sazonov S. Y., Ostriker J. P., Sunyaev R. A., 2004, *MNRAS*, 347, 144

Simpson, C. 2005, *MNRAS*, 360, 565

Spergel D. N., et al., 2003, *ApJS*, 148, 175

Taniguchi Y., et al., 2005, *PASJ*, 57, 165

Wang J. X., Rhoads J. E., Malhotra S., Dawson S., Stern D., Dey A., Heckman T. M., Norman C. A., Spinrad H., 2004, *ApJL*, 608, L21

Wyithe, J. S. B., & Loeb, A. 2002, *ApJ*, 581, 886

Wyithe J. S. B., Loeb A., 2003, *ApJ*, 595, 614

Wyithe J. S. B., Loeb A., 2004, *Nature*, 427, 815

APPENDIX A: TRANSMISSION OF $\text{Ly}\alpha$ PHOTONS FROM AGN

For a source of UV radiation embedded in a neutral IGM the emission blueward of the $\text{Ly}\alpha$ line center is suppressed by a factor of $\langle e^{-\tau_{\text{GP}}} \rangle$. Here, the Gunn-Peterson optical depth, τ_{GP} is given by

$$\tau_{\text{GP}} = \frac{3n(z)A_{\alpha}\lambda_{\alpha}^3}{8\pi H(z)} = 6.4 \times 10^5 \left(\frac{\Omega_b h^2}{0.022} \right) \left(\frac{0.15}{\Omega_m h^2} \right)^{\frac{1}{2}} \left(\frac{1+z}{7.5} \right)^{\frac{3}{2}}, \quad (\text{A1})$$

where $A_{\alpha} = 6.25 \times 10^8 \text{ s}^{-1}$ is the Einstein A coefficient, $\lambda_{\alpha} = 1216 \text{ \AA}$ is the $\text{Ly}\alpha$ wavelength, and $n(z)$ and $H(z)$ are the number density of neutral hydrogen atoms and the Hubble constant at redshift z , respectively (Gunn & Peterson 1965). For photons initially redward of the $\text{Ly}\alpha$ line center, the Gunn-Peterson optical depth reduces to

$$\begin{aligned} \tau_{\text{GP}}(x) &= \tau_{\text{GP}} \frac{1}{\sqrt{\pi}} \int_x^{\infty} \phi(x') dx' \approx -\tau_{\text{GP}} \frac{a}{\pi x} \\ &\approx 10 \left(\frac{1+z}{7.5} \right)^{3/2} \left(\frac{300\text{K}}{T_{\text{gas}}} \right)^{1/2} \left(\frac{-38}{x} \right). \end{aligned} \quad (\text{A2})$$

Here we have expressed the frequency ν in terms of $x \equiv (\nu - \nu_0)/\Delta\nu_D$, where $\Delta\nu_D = v_{th}\nu_0/c$, and $v_{th} = \sqrt{2k_B T/m_p}$ is the thermal velocity of the hydrogen atoms in the gas, k_B is the Boltzmann constant, T the gas temperature, m_p the proton mass and $\nu_0 = 2.47 \times 10^{15} \text{ Hz}$ is the central $\text{Ly}\alpha$ frequency. Note that $x < 0$ for photons redward of the line center. To obtain the simple expression in Eq. (A2), we approximated the Voigt function $\phi(x)$ in the line wing as $\phi(x) = a/[\sqrt{\pi}x^2]$, where a is the Voigt parameter and $a = A_{\alpha}/4\pi\Delta\nu_D = 4.7 \times 10^{-4}$ ($13 \text{ km s}^{-1}/v_{th}$) is the ratio of the Doppler to natural line width.

Another way to write the Gunn Peterson damping wing optical depth is in terms of a velocity offset, Δv . For a photon initially redshifted by Δv relative to the line center, the total Gunn-Peterson optical depth reduces to:

$$\tau_{\Delta v} \approx 10 \left(\frac{1+z}{7.5} \right)^{3/2} \left(\frac{85 \text{ km s}^{-1}}{\Delta v} \right). \quad (\text{A3})$$

Note that this expression is independent of the gas temperature.

Assuming the intrinsic $\text{Ly}\alpha$ spectrum of an AGN to be Gaussian of width $\sigma_v = v_{\text{HWHM}}$ (Eq. 13) with a central flux that is N times the continuum⁴. The intrinsic flux density (in arbitrary units) becomes

$$F(x) = 1 + \frac{N-1}{\sigma_x \sqrt{2\pi}} \exp\left[-\frac{x^2}{2\sigma_x^2}\right], \quad (\text{A4})$$

where $\sigma_x = \sigma_v/v_{th}$. The IGM transmission is given by

⁴ This corresponds to a $\text{Ly}\alpha$ EW of $N \times [2v_{\text{HWHM}}/c] \times \lambda_{\alpha} \text{ \AA} = 200 \times (N/10) \times (v_{\text{HWHM}}/[3000 \text{ km s}^{-1}]) \text{ \AA}$.

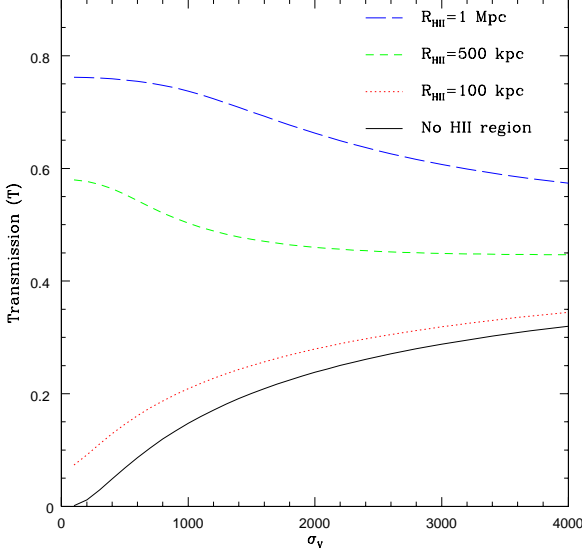


Figure A1. The fraction \mathcal{T} of Ly α photons emitted by a $z = 6.5$ quasar embedded in a neutral IGM, that can freely (unscattered by neutral hydrogen atoms in the IGM) propagate to the observer. The figure shows \mathcal{T} as a function of the intrinsic Ly α line width of the quasar, $\sigma_v = v_{\text{HWHM}}$. Four lines are shown. The figure shows that an IGM transmission of $\mathcal{T} = 0.3$ is accurate to within a factor of 2 for a wide range of parameters.

$$\mathcal{T} = \frac{\int_{-\infty}^{\infty} dx [F(x) - 1] e^{-\tau(x)}}{\int_{-\infty}^{\infty} dx [F(x) - 1]}, \quad (\text{A5})$$

where $F(x)$ and $\tau(x)$ are given by Eq. (A4) and Eq. (A2). The transmission \mathcal{T} is plotted as a function of σ_v in Figure A1 as the *black solid line*.

The other lines represent the IGM transmission in the presence of a cosmological HII region with a radius of 0.1 (*red-dotted line*), 0.5 (*green-dashed line*) and 1.0 Mpc (*blue-long-dashed dotted line*) surrounding the AGN. The radius of the HII region surrounding a quasar of age t_Q powered by a black hole of mass M_{BH} shining at Eddington luminosity is given by (Haiman & Cen 2002)

$$R_{\text{HII,edd}} = 0.74 \left(\frac{M_{\text{BH}}}{10^7 M_{\odot}} \right)^{1/3} \left(\frac{t_Q}{2 \times 10^7 \text{ yr}} \right)^{1/3} \left(\frac{1+z}{7.5} \right) \text{ Mpc}. \quad (\text{A6})$$

This relation assumes the total ionizing luminosity of AGN, L_{ion} , to scale as $L_{\text{ion}} \propto M$. Alternatively, the Kaspi relation shows that the continuum luminosity at $\lambda = 5100 \text{ \AA}$ scales as $\propto M^{1.3}$ (Eq. 11). If the brightest $z > 6$ AGN accrete at the Eddington luminosity, and we assume that the total ionizing luminosity emitted by an AGN also scales as $M^{1.3}$, we get

$$R_{\text{HII,kas}} = 0.44 \left(\frac{M_{\text{BH}}}{10^7 M_{\odot}} \right)^{0.43} \left(\frac{t_Q}{2 \times 10^7 \text{ yr}} \right)^{1/3} \left(\frac{1+z}{7.5} \right) \text{ Mpc}. \quad (\text{A7})$$

The size of the HII region is also determined by the uncertain value of the escape fraction of ionizing photons, f_{esc} . Accounting for these uncertainties, Figure A1 shows that for $\sigma_v = 3000 \text{ km s}^{-1}$, \mathcal{T} lies in the range 0.3–0.45 given

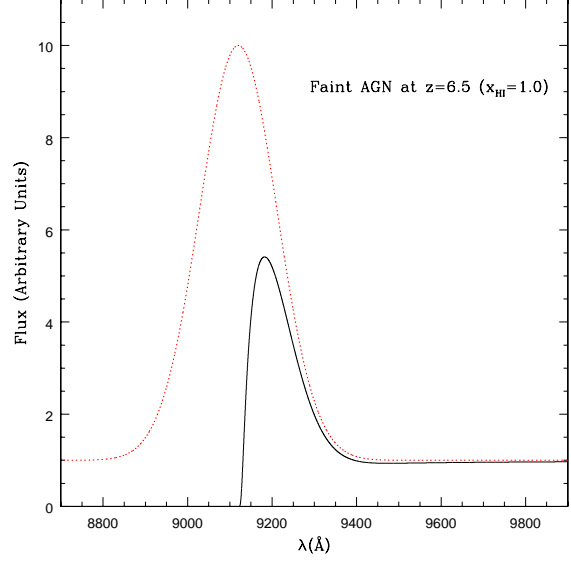


Figure A2. The expected spectrum of a faint AGN at $z = 6.5$ in a neutral IGM (i.e. no cosmological HII region is present). The intrinsic emitted Ly α line of an AGN is shown as the *red dotted line*. A neutral IGM erases a large fraction of the line, transmitting only the reddest photons to an observer. The resulting observed spectrum is shown as the *black solid line*. The figure shows that these AGN have a peak Ly α flux redward of the true line center by $\sim 60 \text{ \AA}$ (corresponding to $\sim 2000 \text{ km s}^{-1}$) and an observed v_{HWHM} that is a factor of ~ 2 times lower than the emitted v_{HWHM} .

$R_{\text{HII}} = 0 - 500 \text{ kpc}$. The range of \mathcal{T} increases towards lower σ_v . However we find that an IGM transmission of $\mathcal{T} = 0.3$ is accurate to within a factor of 2 for a wide range of the parameters σ_v , f_{esc} and total ionizing luminosity.

In Figure A2 the *black solid line* shows the theoretical spectrum of a $z = 6.5$ AGN embedded in a neutral IGM (i.e. no cosmological HII region is present). We assume the black hole mass to be $10^7 M_{\odot}$, which according to Eq. (13) should yield $v_{\text{HWHM}} = 4 \times 10^3 \text{ km s}^{-1}$. However, at low luminosities, and therefore low black hole masses, $v_{\text{HWHM}} \rightarrow 3 \times 10^3 \text{ km s}^{-1}$ (Kaspi et al. 2000). The intrinsic Ly α spectrum (the *red dotted line*) is described by Eq. (A4), in which we assumed $\sigma_v = 3 \times 10^3 \text{ km s}^{-1}$ and $N = 10$ (which yields an Ly α EW of 200 \AA).

We note that the observed line center lies redward of the true line center by $\sim 60 \text{ \AA}$, which translates to $\sim 2000 \text{ km s}^{-1}$. Furthermore, the observed v_{HWHM} is ~ 2 times lower than the emitted value.